Int. J. Environ. Res., 9(3):1055-1068, Summer 2015
ISSN: 1735-6865

Modified Zero valent Iron (ZVI) Nanoparticles for removal of Manganese from water

Agarwal, M.*and Patel, D.

Department of Chemical Engineering, Malaviya National Institute of Technology Jaipur, India

Received 19 Sep. 2014; Revised 26 Dec. 2014; Accepted 26 Dec. 2014

ABSTRACT: Manganese is one of the significant raw materials for various industries and most difficult element to remove from water because of its high solubility. The treatment of Mn (II) contained wastewater is stringent for environmental preservations. In the present study adsorption of Mn^{2+} on Zero-Valent Iron nanoparticles synthesized by chemical reduction process and modified with phosphate coating was investigated. Synthesized nanoparticles were characterized by Scanning Electron Microscopy (SEM), Energy dispersive X-ray spectrometry (EDS), X-ray diffraction (XRD) and Fourier transform infrared spectra (FTIR).The effects of contact time, adsorbent dose, Mn (II) initial concentration, pH and temperature were investigated. The maximum adsorption occurred after 5 hrs and maximum removal (92.45%) of Mn(II) took place at a pH of 9. The removal rates of Mn (II) decreased from 93.11% to 68.82% as the initial concentration was increased from 2 to 9% (approximately) when ZVI nanoparticles were used. On the other hand the removal rate is almost steady when modified ZVI nanoparticles with PO_4^{-3} were used. The equilibrium data fits well to Langmuir adsorption isotherm, suggests monolayer adsorption. The adsorption followed the Pseudo second order kinetics. The effect of other metal ions present in water on the removal of Mn (II) has been also investigated.

Key words: Adsorption, Zero valent Iron, Nanoparticles, Manganese removal

INTRODUCTION

Pollution of water is a serious concern for the mankind with the development of technology. Industries are main sources of pollutions directly or indirectly. Mainly two types of industrial pollutants are present in water coming from the industry wastes. These are organic and inorganic pollutants. Several methods have been invented by researchers to remove organic pollutants like dyes (Gupta *et al.,* 2011, 2012; Mittal *et al.,* 2009, 2010; Karthikeyan *et al.,* 2012;Saleh and Gupta,2012). Water pollution by inorganic pollutants like heavy metal effluents discharged from various industries has now become a major environmental concern. Heavy metal ions such as Zn^{2+}, Cr^{3+}, Cd^{2+}, Pb^{2+}, Mn^{2+}, and Hg^{+} are non-biodegradable, highly toxic and probably have a carcinogenic effect (Rahmanian *et al.*,2011; Gupta and Nayak 2012). Manganese is the 10th most abundant element in the earth's crust and second only to iron as most common heavy metal. Manganese containing effluents come from metallurgical, textile, electroplating, ceramics, dry cell batteries, pigments and paint industries. All of these come under the ground pollution sources. Manganese (II) is present in considerable amount in mine drainage water (Hallberg and Johnson, 2005). Presence of Manganese in water can lead to various health and equipments problems. It affects appearance of water and imparts metallic taste to water. Doses in excess to some critical amount of Mn(II) can cause neurotoxicity to human beings in terms of a syndrome resembling Parkinson's disease as indicated by Roth et al.(2002). It can cause corrosion and pipe blockage (Scholz, 2006).

Bioaccumulation of this metal led United Nations Food and Agriculture Organization recommend maximum level for Manganese in irrigation water to be 0.2 mg/L. The United State Environment Protection Agency (USEPA) and European Commission have specified manganese levels to be within 0.05mg/L in drinking water, while Indian Standard Specification for drinking water allows 0.1mg/L recommended by IS: 3307 (1977). The industrial effluents containing high concentration of Mn(II) pollute not only surface water but also ground water through soil percolation and

*Corresponding author E-mail: madhunaresh@gmail.com

rain. The problem becomes severe in countries like India where ground water is the main source of drinking water. Manganese concentrations up to 0.4mg/L have been measured in wastewater effluent from various industrial effluents in Jaipur (India) (Singh and Chandel, 2006). High manganese concentration (850mg/kg) was reported in the soils distributed in central India (Jaiswal and Patel, 2008). Surface water in China Nigeria was reported to be heavily polluted by manganese (2.054 mg/L) due to effluent discharge from mining, smelting and textile industries (Li *et al.*,2009; Yusuff and Sonibare,2004).

Several methods have been established, in order to remove heavy metals from polluted water such as ion exchange, chemical precipitation, membrane filtration adsorption, coagulation and flocculation, electrochemical treatment, and flotation. Adsorption is accepted as an effective and economic method for the removal of heavy metals (Ponder *et al*., 2000 and Gupta and Nayak, 2012). Adsorption becomes most effective when the surface area of the adsorbents is increased. The application of nanoparticles in this context is, therefore, highly suitable for the environmental remediation and pollutant removal. Functional nanoparticles like MWCNTs are very sensitive to metal ions and could be used as one of the components for sensing poisionous Hg(II) ion (Khani *et al.,* 2010).Gupta *et al.* (2011) found that Alumina-coated multi-wall carbon nanotubes can be used as an effective adsorbent for the removal of lead ions from aqueous solution. Recently, Zero Valent Iron (ZVI) nanoparticles have emerged as very successful agent for the removal of heavy metals due to their high reducing capability surface area and magnetism. It is easier to separate manganese ions adsorbed nanoparticles from the aqueous solution of manganese through magnetic separation. Although, ZVI nanoparticles have been reported to demonstrate effective fixation for various types of metallic ions, including Pb^{2+}, Cr^{6+}, Ni^{2+}, As^{3+}, As^{5+}, Cd^{2+}, Cu^{2+}, Zn^{2+}, Ba^{2+} and Co^{2+} (Li and Zhang,2006;Kanel *et al*., 2005; Kanel *et al*., 2006; Li and Zhang,2007; Celebi *et al.*, 2007; Uzum *et al*., 2008; Kassaee *et al*., 2011) during the last few years no report of the interaction of ZVI with Mn^{+2} is available in literature. Considering the exceptional properties of ZVI nanoparticles as mentioned above present study deals with a comparative adsorption study of Mn^{+2} on Zero-Valent Iron (ZVI) nanoparticles and phosphate ion modified ZVI nanoparticles. The characterization techniques involved are Transmission electron microscopy with energy dispersive spectra (TEM-EDS) analysis and X-ray diffraction (XRD). The adsorption of manganese ions onto ZVI nanoparticles have been carried out in batch equilibrium conditions. The effects of different parameters including contact time, adsorbent dose, pH, initial metal ion concentration and temperature have been investigated also.

MATERIALS & METHODS

Ferrous Sulfate ($FeSO_4.7H_2O$) (Make: Qualigens), sodium borohydrate ($NaBH_4$) (Make: Qualikems), Manganous Sulfate mono hydrate ($MnSO_4.H_2O$) (Make: Rankem), Ethenol (C_2H_5OH) (Make: Merk), Potassium dichromate (K_2CrO_7) (Make: CDH), Zinc Sulfate ($ZnSO_4.7H_2O$) (Make: LobaChemie), lead Sulfate ($PbSO_4$) (Make: CDH), Nitric acid pure (HNO_3) (Make: LobaChemie) etc. were used for the study..
Fe (0) nanoparticles were synthesized by the reduction of iron sulphate (II) with borohydride (Shao-feng *et al.,* 2005) according to reaction (1):

$$4Fe^{+2}(aq) + BH^{-}_{4}(aq) + 3H_2O \;\; ---> \;\; 4Fe^{0}(s) + H_3BO_3(aq) + 7H^{+} \qquad (1)$$

The solution of $NaBH_4$ (0.2M) and $FeSO_4.7H_2O$ (0.05M) were made in 1:1 volume ratio, The solution of $FeSO_4.7H_2O$ (Qualigens, India) (0.05M in a 500 ml beaker) was continuously stirred (magnetic stirrer, 400 rpm) at room temperature. $NaBH_4$ solution was added drop wise from burette (1 ml/min) to the FeSO4.$7H_2O$ solution. Some of zero-valent iron formed is consumed according to reaction (2):

Excess Borohydride was added to the reaction beaker to avoid the following oxidation step (2) (Bhattacharyya and Sharma, 2005):

$$Fe^{0}(s) + 2H^{+} \;\; ---> \;\; Fe^{+2} + H_2(g) \qquad (2)$$

The generated iron nanoparticles were filtered through Whatman filter Paper and stabilized with a large volume of deionized water (>100 mL/g) to wash, and at the end, with diluted ethanol (~5%). Synthesized nanoparticles were dried in hot oven at 50°C for 24 hrs.

Surface modification of the nanoparticles was done by attaching Phosphate group to it. For this purpose initial steps followed were similar to synthesis of ZVI. The solution of $NaBH_4$ (0.2M) and $FeSO_4.7H_2O$ (0.05M) were made in 1:1 volume ratio, then the solution of $FeSO_4.7H_2O$ (in a 250 ml Conical flask) was kept on magnetic stirrer at 400 rpm and room temperature. Now $NaBH_4$ solution was added drop wise from burette at the rate of 1 ml/min in stirring beaker containing $FeSO_4.7H_2O$ solution for 30 minutes. After 30 minutes, 10 ml di-potassium hydrogen orthophosphate (K_2HPO_4) (0.4 g/ml) was added to the reaction mixture. The generated phosphate coated nanoparticles were filtered by Whatman filter Paper and stabilized with a large volume of deionized water (>100 mL/g) to wash, and at the end, with diluted ethanol (~5%). Synthesized nanoparticles were dried in hot Oven at 50°C for 24 hrs.

Scanning electron microscope (Nova Nano FE-SEM 450,FEI) and transmission electron microscope (TEM, a Tecnai G^2 T20 (FEI) S-Twin) were used to analyze the particle size, shape and morphology. Elemental analysis was performed with an Energy Dispersive System (EDS, Bruker) attached to the microscope. Fourier transform infrared spectroscopy (FTIR, perkinelmer spectrum 2) was performed to confirm the presence of the characteristic peaks of the bonds in the nanoparticles. The structural properties of Fe^0 powder was analyzed by X-ray powder diffraction (XRD) of Panalytical, X Pert Pro diffractometer using the monochromatized X-ray beam from the nickel-filtered Cu K radiation.

The batch adsorption experiments were performed first using ZVI nanoparticles to get suitable operating conditions for maximum removal of manganese from water. Once operating conditions were obtained modified nanoparticles were used for manganese removal to check improvement in removal efficiency. The effects of experimental parameters such as adsorbent dose (0.1-5 g/l), initial metal ion concentration (2– 9 mg/L), pH (3–11), temperature (25–50) and Common ion effect on the adsorptive removal of Mn(II) ions were studied in a batch process for a specific period of contact time i. e. equilibrium time (5 hrs.). All adsorption experiments were conducted in 250 mL conical flasks, adding 100 mL of manganese solution (with desired concentration and pH) and desired dose of adsorbent (ZVI nanoparticles), and then mechanically agitating at 200 rpm for the required temperature. After filtration through the Whatman filter paper no. 1, Mn(II) ions remaining in the solution were determined by Atomic Absorption spectroscopy. The amount of adsorbed manganese per gram of ZVI nanoparticles at equilibrium, q_e (mg/g), and the removal percentage, (% removal), were calculated by equations (3, 4) given below:

$$q_e = (C_0 - C_e)/W \quad (3)$$

$$\% \, Removal = (C_0 - C_e)/C_0 \times 100 \quad (4)$$

Where C_0 and C_e are the initial and equilibrium concentrations of Mn(II) in mg/L, respectively. V is the volume of Mn(II) solution (L) and W is the weight of adsorbent (g).

To predict the amount of metal removal from the aqueous solution knowledge of adsorption kinetics and diffusional resistances were needed. Hence, different models such as pseudofirst-order (Purkait *et al*., 2007), pseudo-second-order (Dogan *et al*., 2007), intraparticle diffusion (Purkait *et al.*, 2007), and Elovich kinetic model (Nemr, 2009;Augustine *et al.*,2007;Shin *et al.*,2011) were implemented to examine the adsorption kinetic data.

The linear formula of pseudo-first-order kinetic can be represented as equation (5):

$$log(q_e - q_t) = log(q_e) - k_1 t/2.303 \quad (5)$$

where q_e and q_t are amount of manganese adsorbed per gram of adsorbent at equilibrium and time t respectively. k_1 is adsorption rate constant. A graph of *log (qe - qt)* vs. t should provide a linear relationship if pseudo-first-order kinetics is followed by adsorption process. From the slope and intercept the value of constants k_1 and q_e, can be obtained.

Pseudo- second order kinetic model in the linear integrated rate equation form (6) was used to found its suitability for adsorption process under consideration.

$$\frac{t}{q_t} = \frac{1}{k_2 q_e^{\,2}} + \frac{t}{q_e} \quad (6)$$

The values of *qe* and k_2 (rate constant) can be calculated from the corresponding slope and intercept of the linear plot of t/q_t vs. *t*.

Elovich kinetic model is rate equation, which describes about adsorption capacity, it is commonly stated as

$$\frac{dq_e}{dt} = \alpha e^{-\beta q_t} \quad (7)$$

Integrating the above equation, for simplification we assuming $\beta q_t >> 1$ and applying boundary conditions $q_t = 0$ at $t = 0$ and $q_t = q_t$ at $t = t$, we get

$$q_t = \frac{1}{\beta}\ln(\alpha\beta) + \frac{1}{\beta}\ln(t) \quad (8)$$

The above equation gives a linear relationship when we plotting a graph *qt* vs. *ln(t)* with a slope of $(1/\beta)$ and an intercept of $1/\beta \, ln(\alpha\beta)$. The constants of the model would be calculated from the slope and intercept.

The adsorption process is a multistep process concerning the transportation of solute molecules from the aqueous phase to the surface of the solid particles followed by diffusion of the solute molecules into the interior of the pores. The second-step diffusion is usually a slow process, and is therefore, rate-determining step. The intraparticle diffusion model (Dogan *et al*., 2007; Augustine *et al.*,2007;Shin *et al.*,2011) is represented using the following equation (9):

$$q_t = K_{diff} t^{0.5} + C^* \quad (9)$$

The plot of *qt* vs. $t^{0.5}$ may represents a multi linearity correlation indicating that two or more steps occur during adsorption process. The intraparticle rate

constant K_{dif}, is directly evaluated from the slope of the regression line and C^* by the intercept. The values of C^* provide information about the thickness of the boundary layer.

The adsorption isotherms describe the effect of different initial metal ion concentrations on the amount of metal ion adsorbed on the adsorbent surface, to find the finest equilibrium position in the adsorption process. . To determine the adsorption isotherm, experiments were performed with 100mL Mn(II) ions solution (2 – 9 mg/L) and 0.1g of exactly weighed amount of adsorbent (1g/L) at 25°C. Obtained data were then concerned with the major isotherm models, namely Langmuir and Freundlich isotherms for adsorbent (zero-valent iron nanoparticles). After calculating value of qe, isotherm models were plotted to test the best fit.

The Langmuir isotherm model is mostly used to define the equilibrium adsorption isotherms of homogeneous surfaces (Foo and Hameed, 2010) . This isotherm model assumes that all sites possess equal affinity for the adsorbate (Bakra *et al.*, 2007). In this theory, the adsorption reaches to its maximum level after a complete monolayer formation of adsorbate molecules onto the adsorbent surface. The Langmuir isotherm model (Demirbas and Nas, 2009) is expressed as equation (10) given below;

$$q_e = \frac{q_m b C_e}{1 + b C_e} \tag{10}$$

Langmuir equation may be presented in linearized form as (Eq. 11):

$$\frac{1}{q_e} = \frac{1}{q_m} + \frac{1}{K_L q_m C_e} \tag{11}$$

q_m = maximum adsorption capacity(Langmuir monolayer adsorption capacity)

K_L = Langmuir constant (The energy of adsorption) The constants were calculated from the intercept and the slope of the linear plot of experimental data of*1/ qe*vs.*1/Ce*

The essential characteristics of the Langmuir isotherm can be expressed by separation or equilibrium parameter, a dimensionless constant as per correlation (12):

$$R_L = 1/(1 + K_L Co) \tag{12}$$

R_L describes the nature of the adsorption process as follows:

- R_L=0, Irreversible
- R_L=1, Linear
- R_L>1, Unfavorable
- 0<R_L<1, Favorable

The values of R_L in the range of 0–1 indicate that the adsorption process is favorable for adsorbent.

The Freundlich isotherm speculates the heterogeneity of the surface and that the adsorption occurs at sites with different energy of adsorption. The energy of adsorption is a function of the surface coverage. Equation (13) represents the Freundlich isotherm (Netpradit *et al.*,2003;Benzina, 1990):

$$q_e = K_f C_e^{\frac{1}{n_f}} \tag{13}$$

Here,K_f is the Freundlich constant and n_f is the heterogeneity factor.

The value of K_f is related to the adsorption capacity of the adsorbent and value of $1/n_f$ is related to the adsorption intensity. Linearized Freundlich isotherm model as shown below (Eq.14) was used to determine the values of Freundlich constants from slop and intercepts.

$$log(q_e) = log(K_f) + (1/n_f) log(Ce) \tag{14}$$

The values of enthalpy ΔH and entropy ΔS of adsorption process were calculated from the slope and intercept of the linear van't Hoff plot using the given below linear equation (15):

$$\ln(K_d) = \frac{\Delta S^0}{R} - \frac{\Delta H^0}{RT} \tag{15}$$

Where ΔS^0= entropy change for the process

ΔH^0 = Enthalpy change for the process

R = gas constant

T = absolute temperature

K_d = ratio of q_e and Ce

The change in free energy (ΔG) for the specific adsorption has also been calculated using the equation (16):

$$\Delta G = - RT \ln K_d \tag{16}$$

RESULTS & DISCUSSION

The morphology of particles was examined using SEM (Nova Nano FE-SEM 450[FEI]). Samples were mounted on aluminum stubs using double sided carbon tape. In this examination, data were collected over a selected area of the surface of the sample, and a 2-dimensional image was generated that displayed spatial variations in these properties areas ranging from approximately 1 cm to 5 microns, in width can be imaged in a scanning mode using conventional SEM techniques (magnification ranging from 12000X to approximately 100,000X, spatial resolution of 50 to 100 nm). SEM micrographs [Fig. 1(a) and (b)] show the differences in particle sizes when prepared in different

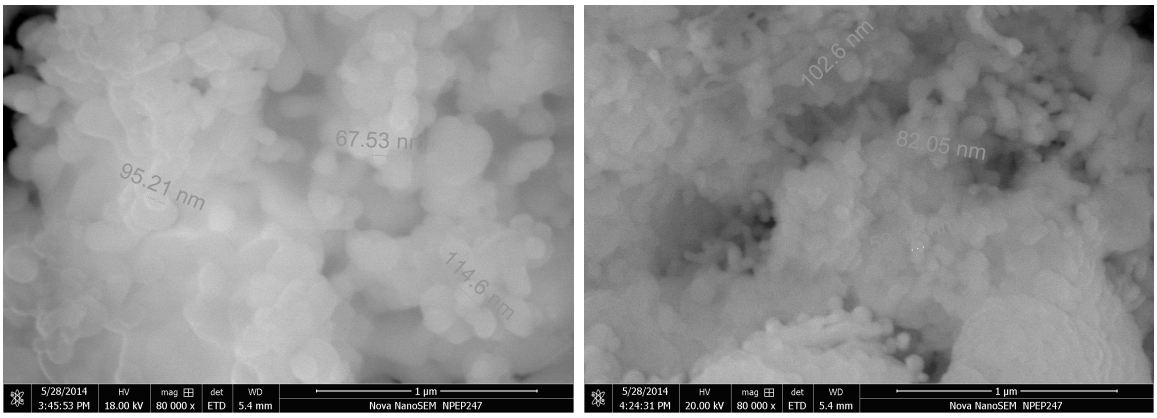

(a) **(b)**

Fig. 1. SEM micrographs of: (a) ZVI nanoparticles and (b)ZVI nanoparticles modified with phosphate group

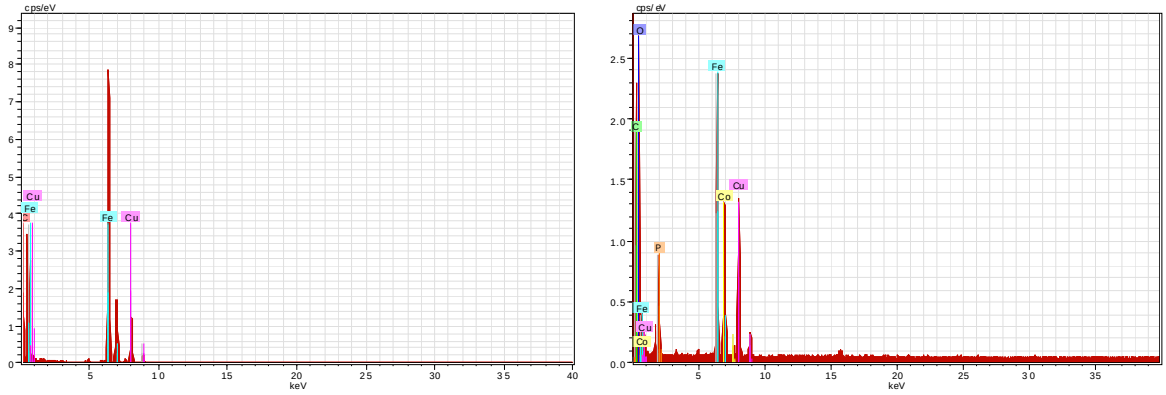

(a) **(b)**

Fig. 2. EDS of: (a) ZVI nanoparticles and (b) Modified ZVI nanoparticles with phosphate group

chemical environments. It is evident that the size of the ZVI particles reduces to a great extent when Phosphate ions are present in the reaction system. The SEM image showed that the particles had spherical morphologically and were agglomerated due to high surface area.

EDS analysis [Fig. 2(a) and (b)] shows that phosphorus is present along with iron.

Formation of Fe^0 has been confirmed from the XRD pattern presented in Fig. 3. Figure 3(a) shows the characteristic XRD pattern with prominent peaks at 2θ of 45°, 65° and 85° typical of Fe^0 crystals. Fig. 3(b) shows that the phosphate groups were attached with the iron as the characteristics Fe peaks has been shifted from its original position and new peaks were also developed. Broadening of peaks in both the Figure 3(a) and 3(b) suggests the presence of low crystallite size in the synthesized ZVI particles. IR-spectra were obtained using a Perkin Elmer spectrum 2 IR-spectrometer (Perkin, Norwalk, USA) Samples were mixed with micronized KBr powder and compressed into discs at a force of 10 kN for 2 min using a manual tablet press. Figure 4(a) shows the FTIR spectra of Fe^0 nanoparticles and figure 4(b) shows FTIR of modified Fe^0 with phosphate group. The doublet obtained at 1042.59 cm^{-1} and 938.25 cm^{-1}shows successful incorporation of phosphate anion with iron. The peaks at 3400 cm^{-1}, 2923 cm^{-1} represent –OH stretching vibrations of water. Similar peaks were also obtained for modified ZVI nanoparticles. The peaks at 584 cm^{-1} (Fig.4a) and at 561 cm^{-1}(Fig.4a) correspond to Fe-O stretching vibrations. Effect of various operating parameters such as time, adsorbent dose, pH, temperature etc. on %manganese removal and adsorbent capacity was estimated using ZVI nanoparticles .

The optimum experimental conditions thus obtained were used for modified ZVI nanoparticles.

Batch experiments as per sec. 2.5 were carried out and variation of Mn(II) concentration in terms

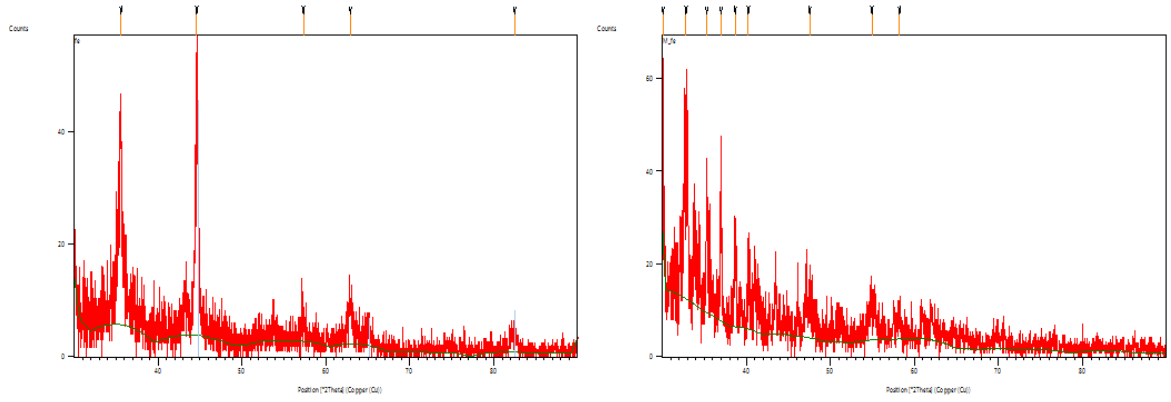

(a) **(b)**

Fig. 3. XRD pattern of: (a) ZVI nanoparticles and (b) Modified ZVI nanoparticles with phosphate group

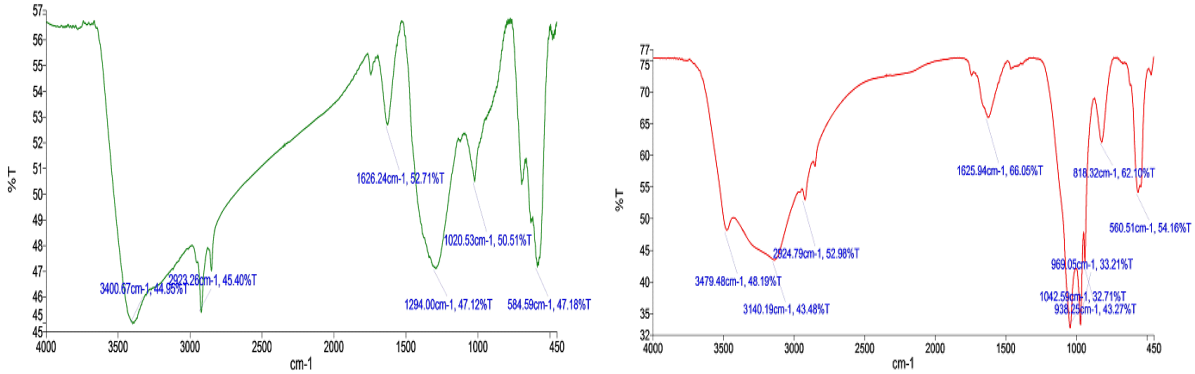

(a) **(b)**

Fig. 4. FTIR spectra of: a) ZVI nanoparticles and (b) Modified ZVI nanoparticles with phosphate group

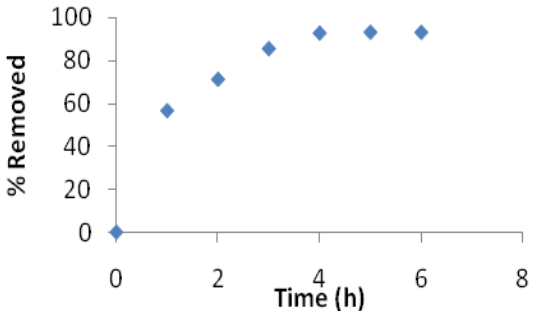

Fig. 5. Percent Removal of Manganese at different time interval for adsorption onto ZVI Nanoparticles (dose = 1 g/L; Initial Mn(II) conc. = 2 mg/L, Temperature 25°C)

of % removal from the solution as a function of time with iron zero nanoparticles (1g/L) was shown in Fig. 5. It can be seen from the figure that the percent removal of Mn(II) from water had increased gradually with time from 55% to 93% and then stabilized. After 5 hrs of operation there was no appreciable increase in % removal was observed. This implied that the nanoparticles had reached its maximum adsorption capacity in 5 hrs and thereafter get saturated. Hence, 5 hrs of treatment time was used in all subsequent experiments as batch equilibrium time. Batch adsorption experiments were carried out for obtaining optimum adsorbent dose for manganese removal from water.

The effect of adsorbent dose on removal of Mn(II) was examined with adsorbent dose in the range of 0.1–5g/L at 25°C, with an initial Mn(II) concentration of 2 mg/L (Fig. 6a). As shown in Fig. 6, the quantity of Mn(II) adsorbed had increased from around 75% to 93% when adsorbent dose was increased from 0.1 to 5g/L because of the availability of larger surface area and adsorption sites. At a dose of 1 g/L, maximum percent removal was obtained.

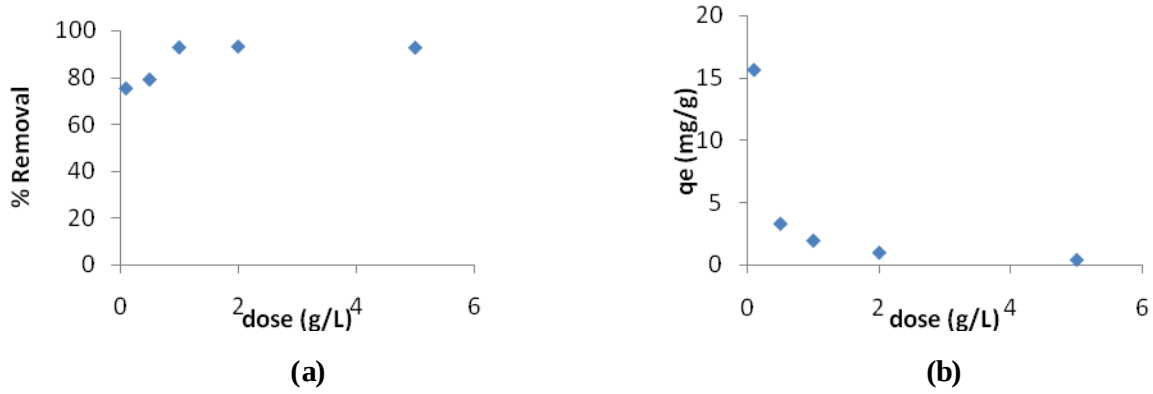

Fig. 6. (a) Percent Removal and (b)adsorption capacity (qe) of Manganese at different dosage of ZVI Nanoparticles (dose = 0.1-5 g/L; Initial Mn(II) conc. = 2mg/L, Temp. 25°C)

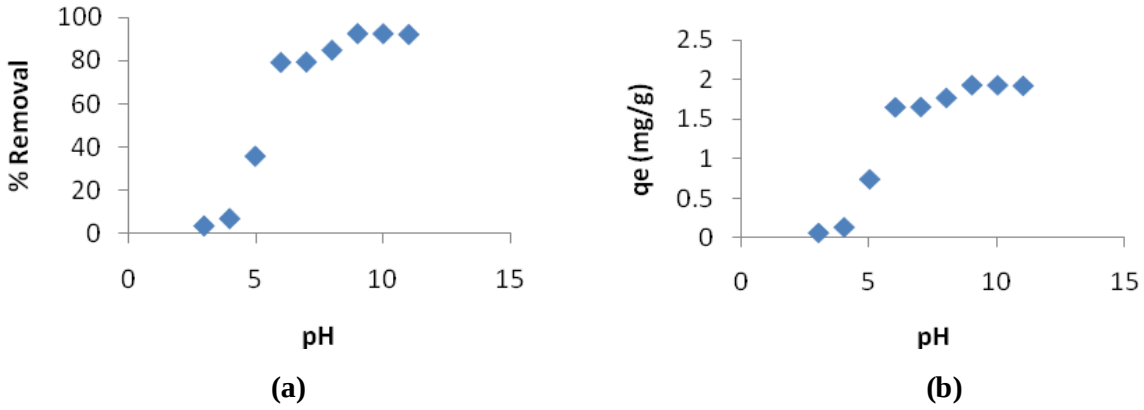

Fig. 7. (a) Percent Removal and (b) adsorption capacity (qe) of Manganese at different pH for adsorption onto ZVI Nanoparticles (dose = 1 g/L; Initial Mn(II) conc. = 2 mg/L, Temp. 25°C)

Fig 6(b) shows the graph between adsorption capacity (qe) and adsorbent dose (g/L). Initially, when adsorbent dose was 0.1g/L the adsorption capacity was maximum at 15.61 mg/g and further upon increasing the dose the adsorption capacity decreases. The reason for such behavior may be attributed to the fact that upon increasing the dose, more sites were available for same amount of manganese, leading to unsaturation of adsorbent sites.

It was observed that the pH of the solution had great influence on adsorption of heavy metal ions from aqueous solutions. Fig. 7 shows the effect of pH (range3-11) on the removal of Mn(II) ions by zero-valent iron nanoparticles from aqueous solutions. The removal of Mn(II) increased with increase in pH up to 9, thereafter no noticeable change was observed. The Mn(II) removal was 78% at pH 7 and it was 92.45% at pH 9. The maximum removal percentage occurs at pH = 9 and hence it was taken as the optimum value for further adsorption studies. Similarly the adsorption capacity (qe) was maximum at pH = 9 for Mn(II) as shown in Fig. 7(b).Most of adsorption processes for removal of pollutant species from aqueous solutions being exothermic in nature. The exothermic metal removal process get affected with operating temperature, therefore, a series of experiments were conducted at various operating temperature. The results obtained were shown in Fig. 8(a) and 8(b). No significant effect on Mn(II) percent removal and adsorption capacity (qe) of Mn(II) was observed by increasing the temperature from 25 to 30°C but further increasing the temperature from 30 to 50°C the removal percentage of Mn(II) decreased from around 93% to 23% and the adsorption capacity also decreases 1.93 to 0.49 mg/g (Fig. 8a,b). Less adsorption at higher temperature may be due to increased solubility of manganese in the solution along with desorption from the adsorbent surface.

From above experiments the suitable operating conditions obtained for maximum removal of

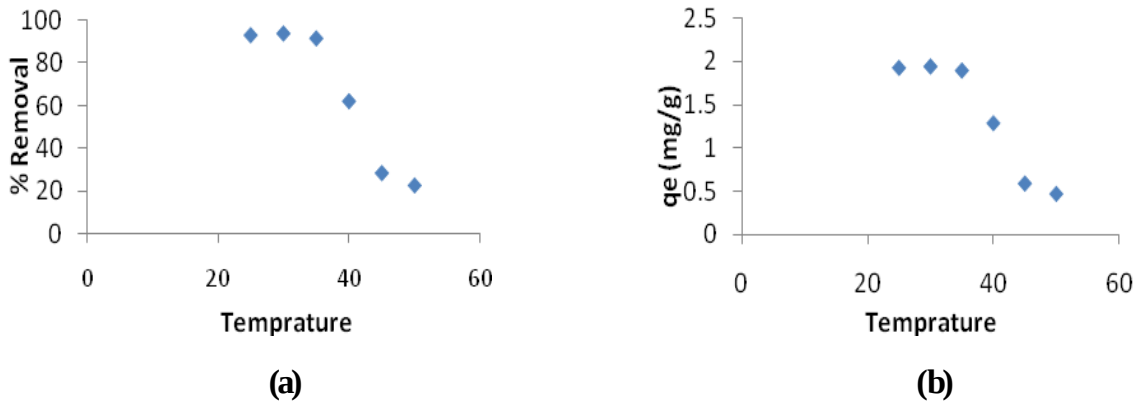

(a) **(b)**

Fig. 8. (a) Percent Removal and (b) adsorption capacity (qe) of Manganese at different temperatures for adsorption onto ZVI Nanoparticles (dose = 1 g/L; Initial Mn(II) conc. = 2 mg/L)

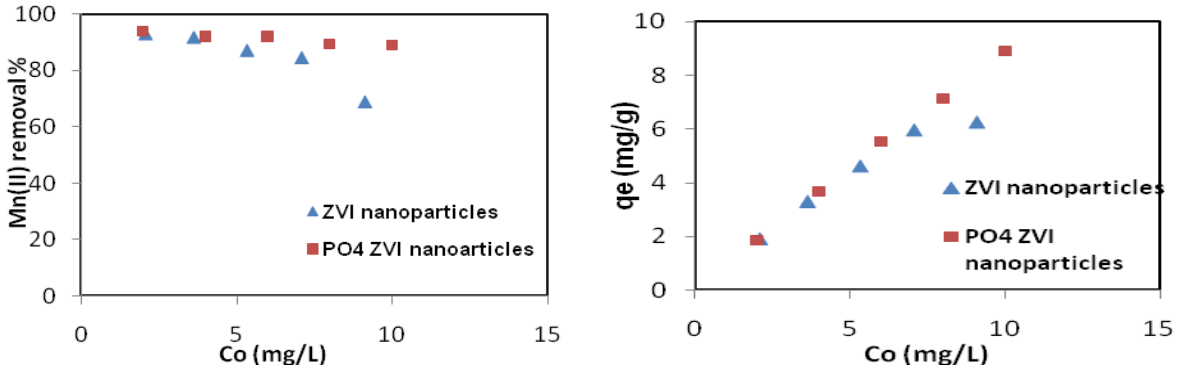

(a) **(b)**

Fig. 9. (a) Percent Removal and (b) adsorption capacity (qe)of Manganese at different initial conc. for adsorption onto ZVI nanoparticles and PO_4 coated modified ZVI Nanoparticles (dose = 1 g/L; Initial Mn(II) conc. = 2-12 mg/L, Temp. 25°C, pH=9)

manganese by ZVI nanoparticles from aqueous solution were time 5hrs, adsorbent dose, 1g/L, pH 9 and temperature 25°C.

These conditions were used to examine efficiency of modified nanoparticles in removing Mn (II). The effect of the initial concentration of Mn(II) ion solution on adsorption was investigated in the range 2.076 to 9.11 mg/L for ZVI nanoparticles and 2 to 12 mg/L for phosphate coated ZVI nanoparticles. The results are shown in Fig. 9(a) and 9(b). As the initial metal ion concentration increased the percent removal also increased. The fixed dose of nanoparticles have limited adsorption sites, thus, leading to a decrease in percentage removal of heavy metals corresponding to an increased initial Mn(II) ion. The removal rates of Mn (II) was 93.11% when the initial concentration of Mn was 2.076 mg/L and its removal percentage decreased upto 68.82% as the initial concentration was kept at 9.11 mg/L, while the adsorption capacity of adsorbent increased with increase in initial ion concentration.

In the case of phosphate coated ZVI nanoparticles there is small decrease in percentage removal, as it decreases from 94% to 90.65% when increasing the initial concentration from 2 mg/L to 12 mg/L. This reflects that phosphate coated ZVI nanoparticles were more efficient in removing manganese from water. This difference in percent removal was due to $PO4^{-3}$ group that attracted the Mn^{+2} ions from solution and retains them on the surface. The adsorption capacity (qe) saturates in case of ZVI nanoparticles at higher initial concentration(9.11mg/L) of Mn^{+2} while in case of phosphate coated ZVI nanoparticles the adsorption capacity was continuously increasing with initial Mn^{+2} concentration . This difference may be due to presence of phosphate group or structural changes in the adsorbent.

Table 1. Effect of other metal ions on adsorption of Mn(II)

Solution of metal ions	Conc. before adsorption (mg/L)	Conc. after adsorption (mg/L) on ZVI	Conc. after adsorption (mg/L) on modified ZVI	% Removal by ZVI nanoparticles	% Removal by modified ZVI nanoparticles
Mn	1 mg/L	0.157 mg/L	0.041 mg/L	83.3	95.9
Mn + Zn	1 mg/L + 1 mg/L	0.254 mg/L +0.537mg/L mg/L	0.202 mg/L + 0.423mg/L	74.6 + 46.3	79.8 + 57.7
Mn + Cr	1 mg/L + 1 mg/L	0.356 mg/L + Nil	0.130 mg/L + 0.560 mg/L	64.4 + 100	87 + 44
Mn + Zn + Cr	1 mg/L + 0.5 mg/L + 0.5 mg/L	0.413 mg/L + 0.196 mg/L + Nil	0.312mg/L + 0.166mg/L + 0.415mg/L	58.7 + 60.8 + 100	68.8 + 66.8 + 17

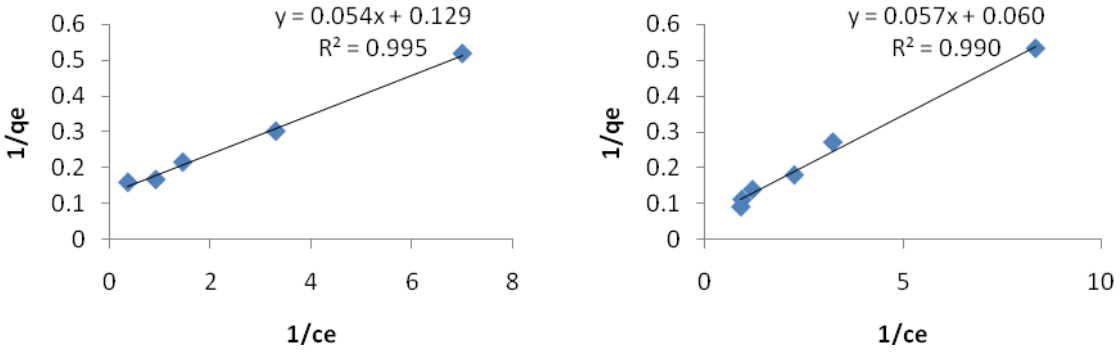

(a) **(b)**

Fig. 10. Langmuir isotherm fitting for adsorption of Mn(II) on (a) ZVI nanoparticles and (b) phosphate coated modified ZVI nanoparticles (dose=1g/L, temperature=25ÚC, Initial Mn(II) conc. =2.076 mg/L).

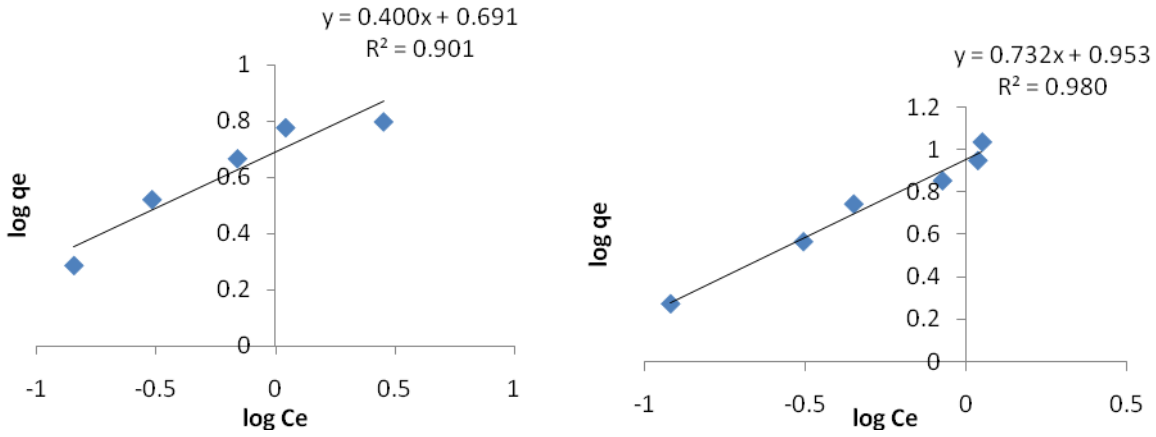

(a) **(b)**

Fig. 11. Freundlich isotherm fitting for adsorption of Mn(II) on (a) ZVI nanoparticles and (b) phosphate coated modified ZVI nanoparticles (dose=1g/L, temperature=25ÚC, Initial Mn(II) conc. =2.076 mg/L).

The effect of other ions on Mn removal by ZVI nanoparticles and phosphate coated ZVI nanoparticles was also analyzed and results obtained were shown in Table 1. From table it can be seen that other metal ions shows competition with manganese for adsorption onto the surface of ZVI nanoparticles and phosphate coated modified ZVI nanoparticles. A drastic reduction in adsorption can be seen when Cr was present in case of ZVI nanoparticles but same was not true for modified ZVI nanoparticles. Table 1 indicates that modified

Table 2. Langmuir, Freundlich isotherm constants, R_L and correlation coefficients for the adsorption of Mn(II) on ZVI and modified ZVI nanoparticles

Isotherms	q_m (mg/g)	K_L (L/mg)	K_f (mg/g)	$1/n_f$	R_L	R^2
Langmuir isotherm						
ZVI nanoparticles	7.71	2.36	-	-	0.17	0.995
Phosphate coated modified ZVI nanoparticles	16.52	1.19	-	-	0.29	0.990
Freundlich isotherm						
ZVI nanoparticles	-	-	4.91	0.40	-	0.901
Phosphate coated modified ZVI nanoparticles	-	-	8.99	0.73	-	0.980

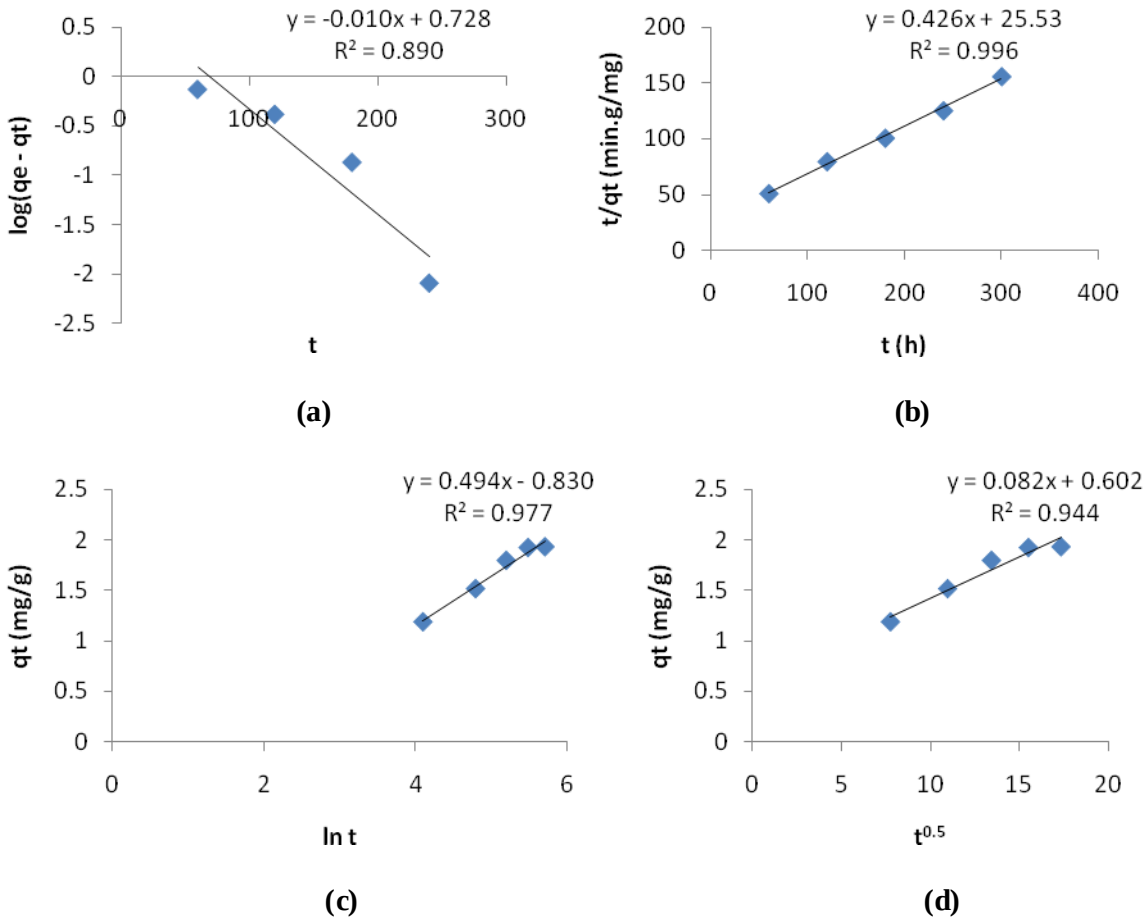

Fig. 12. Kinetic model fitting (a) pseudo first order kinetic model (b) pseudo second order kinetic model (c) Elovich model (d) intraparticle diffusion model for ZVI nanoparticles

nanoparticles are better adsorbent for manganese in presence of other metal ions under consideration.

A plot of 1/qe vs 1/Ce and log (qe) vs log(Ce) were plotted to fit the experimental data to Langmuir isotherm and Freundlich isotherm models respectively for both ZVI and modified ZVI. The linearized plots were shown in Fig. 10(a,b) and 11(a,b). The data fits well to the Langmuir isotherm model for both the adsorbents with correlation coefficient (R^2) in the range 0.99-0.995.The values of maximum adsorption capacities (q_m) were calculated and reported in Table 2. It can be seen from table, that the modified ZVI had higher adsorption capacity (16.54 mg/g) for Mn(II) compared to ZVI (7.71 mg/g). The value of separation factor, R_L reported in Table 2 revealed that adsorption can be considered as favourable.

The kinetics of adsorption process was examined by four kinetic models as stated in section 2. Parameters

Table 3. Kinetic models and their statistical parameters at 25°C

Kinetic models	Parameters	Mn(II)
Pseudo-first order	k_1 (1/min)	0.025
	$q_{e,cal}$ (mg/g)	5.350
	$q_{e,exp}$ (mg/g)	1.927
	R^2	0.89
Pseudo-second order	k_2(g/mg/min)	0.007
	$Q_{e,cal}$ (mg/g)	2.35
	$Q_{e,exp}$ (mg/g)	1.927
	R^2	0.996
Elovich Equation	α (mg/g/min)	0.46
	β (g/mg)	2.24
	R^2	0.977
Intraparticle diffusion	K_{diff}(mg/g/min)	0.082
	C	0.603
	R^2	0.944

Fig.13. The plots of lnK vs. 1/T for adsorption of Mn(II) onto iron nanoparticles

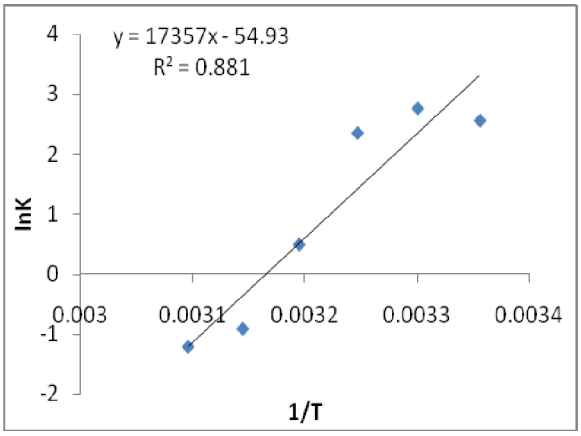

Table 4. Comparison of Adsorption Capacity of Various adsorbents for Mn(II) removal from Water

Adsorbent used	Adsorption capacity, q_{max} (mg/g)	References
Sugarcane bagasse (SCB)	0.676	Esfandiar *et al.*, 2014
Activated carbon(AC)	1.897	
Oxidised multiwall carbon nanotube	3.35	Ganeshan *et al.*, 2013
MnO_2	14	Aguiar *et al.*, 2013
Crab shell chitin (pure)	0.981	Lora and Brennan, 2010
Crab shell chitin with protein	5.437	
NaCl treated natural zeolite tuff	10	Rajic *et al.*, 2009
Clinoptilolite (natural zeolite)	7.69	Doula,2006
Activated carbon immoboilized by tanic acid	1.73	Ucer *et al.*, 2006
Granular activated carbon	2.54	Jusoh *et al.*, 2005
ZVI nanoparticles	7.71	Present Study
Modified ZVI nanoparticles	16.52	Present study

of the kinetic models and regression coefficients (R^2) were calculated from graphs [Fig. 12 a-d] to determine the conformity of the models for the experimental data and were reported in Table 3. The higher value of regression coefficients (0.996) confirms the applicability of pseudo-second order kinetics. The values $q_{e,cal}$ and $q_{e,exp}$. were also close in case of pseudo-second order kinetic model. Therefore, it can be identified that absorption kinetics well characterized by pseudo-second order kinetic model signifying chemisorption behavior.

Intraparticle diffusion model was also examined to determine the controlling mechanism in adsorption kinetics. Since the plot of q vs. $t^{1/2}$ [Fig.11(d)] did not pass through origin, intraparticle diffusion cannot be considered as the sole rate-controlling step.

From temperature vs % removal graph (Fig. 13), it can be seen that the removal of Manganese from water was higher at lower temperatures and decreases on increasing the temperature, indicating the exothermic nature of adsorption. The prediction was further confirmed by the value of enthalpy change (ΔH^0= -144 KJ/mol) calculated using Van't Hoff equation. Curves were plotted with lnK as ordinate and 1/T as abscissa for adsorption of Mn(II) on iron zero nanoparticles as shown in Fig 13.

From adsorption studies of Manganese using nanoparticles, it was found that value of Gibb's free energy was negative (-6342.02 kJ/mol) at lower temperature (298K) and positive (3241.03 kJ/mol) at high temperatures (323K). This suggests that the process is spontaneous at lower temperatures and exhibits exothermicity.

The adsorption capacity of modified ZVI nanoparticles was compared with other reported adsorbents in the literature and shown in table 4. The Variation in adsorption capacities of various adsorbents may be due to their nature, surface structure, associated functional groups and morphology. The maximum adsorption capacities shown in the table 4

were taken from Langmuir isotherm. It is evident from the comparison that PO_4^{-3} modified ZVI nanoparticles adsorbs higher amount of Mn^{+2} from water than other reported adsorbents.

CONCLUSIONS

Zero-valent iron nanoparticles were synthesized as an adsorbent for manganese removal from water. Maximum removal 92.45% of manganese was obtained with an optimal dose of 1 g/L of ZVI nanoparticles at pH 9 and temperature 25°C. Equilibrium was achieved practically in 300 min. Phosphate coated modified ZVI nanoparticles were also synthesized and used for manganese removal at above operating conditions. Modified nanoparticles showed better efficiency (16.52mg/g) for manganege removal (94%). Adsorption followed Langmuir isotherm in case of both ZVI nanoparticles and Phosphate coated modified ZVI nanoparticles. Adsorption process was better performed at low temperature (30°C) means process is exothermic which was confirmed by Thermodynamics study. High value of heat of adsorption suggests chemisorption. Adsorption kinetics confirms the applicability of pseudo-second order kinetic model. It was found that intraparticle diffusion was not only factor that controlled the adsorption process. Elovich kinetic constants indicated that initial adsorption rate was always less than desorption rate. Process was also feasible and spontaneous.

Overall, it can be concluded that ZVI nanoparticle and modified ZVI could be effectively used as adsorbent for the removal of manganese from its aqueous solution. The results obtained in the study can further be utilized in designing the wastewater treatment plants for the removal of manganese along with other metal ions.

Nomenclature

q_e - Adsorption capacity at equilibrium (mg/g)
q_t - Adsorption capacity at timet(mg/g)
k_1 - Pseudo-first-order rate constant of adsorption (min^{-1})
k_2- Pseudo-second-order rate constant of adsorption (g/mg min)
C^*- thickness of boundary layer
K_{dif} - intraparticle diffusion rate constant (mg/g min)
q_e,*calc* -adsorption capacity at equilibrium calculated for kinetics (mg/g)
q_m - max adsorptioncapacity (mg/g), adsorption capacity at equilibrium determined by experiments
Ce - equilibrium concentration of the adsorbate (mg/L)
K_L - Langmuir constants (L/mg)
C_0 - initial concentration of adsorbate (mg/L)
ΔGÚ- Gibb's free energy (kJ/mol)
Δ*HÚ* - enthalpy change (kJ/mol)
Δ*SÚ* - entropy change (kJ/molK)
R_L -separation factor
T - Temperature in K
Ea - Arrhenius activation energy (kJ/mol)
A - Arrhenius factor
R - Universal gas constant

REFERENCES

Aguiar, A.O., Duarte, R.A., Claudia,A. and Ladeira, Q. (2013). The application of MnO_2 in the removal of Manganese from acid mine water. Water air soil pollution, **224,** 1690-1697.

Augustine, A. A., Orike, B. D. and Edidiong, A.D. (2007). Adsorption kinetics and modeling of Cu (II) ion sorption from aqueous solution by mercaptoacetic acid modified cassava (manihotsculentacranz) wastes. EJEAFChe, **6,** 2221-2234.

Barka. N., Assabbane, A., Nounah, A., Laanab, L. and Ichou, Y. A. (2009). Removal of textile dyes from aqueous solutions by natural phosphate as a new adsorbent. Desalination, **235,** 264-275.

Benzina, M. (1990). Contribution to Kinetics and Thermodynamics Study of Organic Vapors Adsorption on Local Clays, Modeling a Fixed Bed Adsorber. Thesis, University of Sciences, Tunis.

Bhattacharyya, K. G. and Sharma, A. **(**2005). Kinetics and thermodynamicsof Methylene Blue adsorption on Neem (Azadirachtaindica) leaf powder. Dyes Pig., **65,** 51-59.

Celebi, O., Üzüm, C., Shahwan, T. and Erten, H. N. (2007). A radiotracer study of the adsorption behavior of aqueous Ba^{2+} ions on nanoparticles of zero-valent iron. J. Hazard. Mater., **148,** 761-767.

Demirbas, E. and Nas, M. Z. **(**2009). Batch kinetic and equilibrium studies of adsorption of Reactive Blue 21 by fly ash and sepiolite. Desalination, **243,** 8-21.

Dogan, M., Ozdemir, Y. and Alkan, M. (2007). Adsorption kinetics and mechanism of cationic methyl violet and methylene blue dyes onto sepiolite. Dyes Pig., **75,** 701-713.

Doula, M. (2006). Removal of Mn^{+2} ions from drinking water by using clinoptilolite and a clinoptilolite–Fe oxide system. Water Research, **40,** 3167–3176.

Esfandiar, N., Nasernejad, B. and Ebadi, T. (2014). Removal of Mn(II) from groundwater by sugarcane bagasse and activated carbon (a comparative study): Application of response surface methodology (RSM). J. Indust. Engg.Chem., **20,** 3726–3736.

Foo, K. Y. and Hameed, B. H. **(**2010). Insights into the modeling of adsorption isotherm systems. Chemical Engineering Journal, **156,** 2-10.

Ganesan, P., Kamaraj,R., Sozhan, G. and Vasudevan, S. (2013).Oxidized multiwalled carbon nanotubes as adsorbent for the removal of manganese from aqueous solution. Environ. Sci. Pollut. Res., **20,**987–996.

Gupta, V. K., Agarwal, S. and Saleha, T. A. (2011). Synthesis and characterization of alumina-coated carbon nanotubes and their application for lead removal. J. Hazard. Mater., **185,**17–23.

Gupta, V.K., Jain, R., Nayak, A., Agarwal,S. and Shrivastava, M.(2011). Removal of the hazardous dye—Tartrazine by photodegradation on titanium dioxide surface. Materials Science and Engineering, **C 31,** 1062–1067.

Gupta, V.K. and Nayak, A. (2012).Cadmium removal and recovery from aqueous solutions by noval adsorbents prepared from orange peel and Fe_2O_3 nanoparticles. Chemical Engg. Journal,**180,**81-90.

Gupta, V.K., Jain, R., Mittal, A.,Saleh. T.A., Nayak, A., Agarwal, S. and Sikarwar,S.(2012). Photo-catalytic degradation of toxic dye amaranth on TiO2/UV in aqueous suspensions. Materials Science and Engineering, **32,** 12–17.

Hallberg, K. B. and Johnson, D.B. **(**2005). Biological manganese removal from acid mine drainage in constructed wetlands and prototype bioreactors. Sci. Total Environ.,338, 115-124.

Jaiswal, N. K. and Patel, K. S. (2008). Manganese soil pollution in Central India. Goldschmidt Conf. Abstr., A422, Netherlands, **goldschmidt**.info/**2008**/**abstracts**/J.pdf.

Jusoh,A.B., Cheng, W.H. , Low, W.M. , Nora'aini, A. and Megat Mohd Noor, M.J.(2005). Study on the removal of iron and manganese in groundwater by granular activated carbon. Desalination, **182,** 347–353.

Kanel, S. R., Greneche, J. M. and Choi, H. **(**2006). Arsenic (V) removal from ground water using nano scale zero-valent iron as a colloidal reactive barrier material. Environ. Sci. Technol., **40,** 2045-2050.

Kanel, S. R., Manning, B., Charlet, L. and Choi, H. (2005). Removal of arsenic(III)from groundwater by nanoscale zero-valent iron. Environ. Sci. Technol., **39,** 1291-1298.

Karthikeyan, S., Gupta, V.K., Boopathy, R., Titus, A. and Sekaran, G. (2012). A new approach for the degradation of high concentration of aromatic amine by heterocatalytic Fenton oxidation: Kinetic and spectroscopic studies. Journal of Molecular Liquids, **173,** 153–163.

Kassaee, M. Z., Motamedi, E., Mikhak, A. and Rahnemaie, R. **(**2011). Nitrate removal from water using iron nanoparticles produced by arc discharge vs. reduction. Chemical Engineering Journal, **166,** 490-495.

Khani, H., Rofouei, M.K., Arab,P., Gupta,V.K. and Vafaei,Z. (2010). Multi-walled carbon nanotubes-ionic liquid-carbon paste electrode as a super selectivity sensor: Application to potentiometric monitoring of mercury ion(II). J. Hazard. Mater., **183,** 402–409.

Li, X. Q. and Zhang, W. X. (2006). Iron nanoparticles: the core–shell structure andunique properties for Ni(II) sequestration. Langmuir, **22,** 4638-4642.

Li, X. Q. and Zhang, W. X. (2007). Sequestration of metal cations with zerovalentiron nanoparticles—a study with high resolution X-ray photoelectron spectroscopy (HR-XPS). J. Phys. Chem., **C 111,** 6939-6946.

Li, Z., Imaizumi, S., Katsumi, T., Inui, T., Tang, X. and Tangl, Q. (2009).Metal pollution in Huayuan River in Hunan Province in China by manganese sulphate waste residue. Bull. Environ. Contam. Toxicol., **83,** 4583-4590.

Lora,M.A.R. and Brennan, R. A. (2010). Biosorption of manganese onto chitin and associated proteins during the treatment of mine impacted water. Chemical Engineering Journal, **162,** 565–572.

Mittal,A., Kaur,D., Malviya, A., Mittal, J. and Gupta, V.K. (2009). Adsorption studies on the removal of coloring agent phenol red from wastewater using waste materials as adsorbents. Journal of Colloid and Interface Science, **337,** 345–354.

Mittal,A., Mittal, J., Malviya, A. and Gupta, V.K. (2010). Removal and recovery of Chrysoidine Y from aqueous solutions by waste materials. Journal of Colloid and Interface Science, **344,** 497–507.

Nemr, A. E. **(**2009). Potential of pomegranate husk carbon for Cr (VI) removal from wastewater: Kinetic and isotherm studies. J. Hazard. Mater., **161,** 132-141.

Netpradit, S., Thiravetyan, P. and Towprayoon, (2003). Application of waste metal hydroxide sludge for adsorption of azo reactive dyes. Water Res., **37,** 763-722.

Ponder, S. M., Darab, J. G. and Mallouk, T. E. **(**2000). Remediation of Cr(VI) and Pb(II)aqueous solutions using nanoscale zero-valent iron. Environ. Sci. Technol., **34,** 2564-2569.

Purkait, M. K., Maiti, A., Gupta, S. D. and De, S. **(**2007). Removal of congored using activated carbon and its regeneration. J. Hazard.Mater., **145,** 287-295.

Rahmanian, B., Pakizeh, M., Mansoori, S. A. A. and Abedini, R. **(**2011). Application of experimental design approach and artificial neural network (ANN) for the determination of potential micellar-enhanced ultrafiltration process. J. Hazard. Mater., **187(1),** 67-74.

Rajic,N., Stojakovic, D., Jevtic, S., Logar,N.Z., Kovac, J. and Kaucic,V. (2009). Removal of aqueous manganese using the natural zeolitic tuff from the Vranjska Banja deposit in Serbia. J. Hazard. Mater., **172,** 1450–1457.

Roth, J. A., Horbinski, C., Higgins, D., Lein, P. and Garrick, M. D. (2002). Mechanisms of manganese-induced rat pheochromocytoma (PC12) cell death and cell differentiation. Neurotoxicology, **23,** 147-157.

Saleh, T. A. and Gupta, V. K.(2012). Photo-catalyzed degradation of hazardous dye methyl orange by use of a composite catalyst consisting of multi-walled carbon nanotubes and titanium dioxide. Journal of Colloid and Interface Science, **371,** 101–106.

Scholz, M. (2006). Wetland Systems to Control Urban Runoff. Elsevier, 1st edition,131-132.

Shao-feng, N., Yong, L., Xin-hua, X. U. and Zhang-hua, L. (2005). Removal of hexavalent chromium from aqueous

solution by iron nanoparticles. Joumal of Zhejiang University SCIENCE, **6B(10),** 1022-1027.

Shin, K. Y., Hong, J. Y. and Jang. J. (2011). Heavy metal ion adsorption behavior in nitrogen-doped magnetic carbon nanoparticles: Isotherms and kinetic study. J. Hazard. Mater., **190,** 36-44.

Singh, V. and Chandel, C. P. S. (2006). Analytical study of heavy metals of industrial effluents at Jaipur, Rajasthan (India). Journal of Envir. Science & Engineering, **48(2),** 103-108.

Üçer, A., Uyanik, A. and Aygün, ª.F. (2006). Adsorption of Cu(II), Cd(II), Zn(II), Mn(II) and Fe(III) ions by tannic acid immobilised activated carbon. Sep. Purif. Technol., **47,** 113–118

Uzum, C., Shahwan, T., Eroglu, A. E., Lieberwirth, I., Scott, T. B. and Hallam, K. R. **(**2008). Application of zero-valent iron nanoparticles for the removal of aqueousCo^{2+} ions under various experimental conditions. Chemical Engineering Journal, **144,** 213-222.

Yusuff, R. O. and Sonibare, J. A. (2004). Characterization of textile industries effluents in Kaduna, Nigeria and pollution implications. Global Nest: The International Journal, **6 (3),** 211-220.